11 Frequency– and time–dependent effects

11.1 Single wires

11.1.1 Photoconductivity

Irradiation of a 2DEG at the interface of a semiconductor heterostructure may lead to *persistent photoconductivity* via two different mechanisms. First, electron–hole pairs may be generated in the bulk material and charge separation by the electric field at the interface prevents recombination. Second, electrons may be excited from traps located in the doped bulk material. As a consequence of these two processes, the number of carriers available for transport increases and the resistance drops. When the light source is removed, the photoconductivity decays slowly (approximately logarithmically) with time. As disordered conductors in 1D and 2D undergo a conductance change of the order of e^2/h when a single impurity is moved by a distance $\approx \lambda_F$ (see Section 11.1.4 on page 285) the photoconductance may oscillate randomly as a function of time (see for example [89B4, 91L2, 93L4] and references therein).

Bykov et al [89B4] investigated photoconductivity in GaAs samples ($w = 0.2 - 0.5\,\mu$m, $L = 1 - 2\,\mu$m) by exposing them to a LED (maximum at $\lambda = 670\,$nm). They measured $\Delta\sigma$ as a function of time at $T = 1.7\,$K (Fig. 291), it oscillated aperiodically in time. These oscillations persisted for a certain time after the light was turned off. The frequency of the fluctuations increased with the number of incident photons, n_{ph}, and saturated at $n_{ph} \approx 3 \times 10^9\,\mathrm{cm^{-2}s^{-1}}$ (Fig. 292). The Fourier spectrum contained several frequencies, the amplitude of the Fourier components increased with decreasing frequency. The average amplitude of the oscillations increased with increasing n_{ph} and with decreasing temperature. Bykov et al discussed their results in terms of charge exchange involving a number of impurities of the order of unity.

Bykov et al [90B3] measured the four–probe photoconductivity of GaAs samples ($w = 0.5 - 1.0\,\mu$m $L = 2 - 3\,\mu$m) at $6 - 80\,$GHz and $T = 1.4\,$K. As a function of magnetic field it oscillated aperiodically with respect to a positive background and changed sign at some values of B. The character of the oscillations changed with the frequency of the applied radiation. A value for the electron correlation energy was obtained by comparison of the amplitudes of the photoconductivity and the photovoltaic effect.

Bykov et al [91B4] investigated the fluctuation properties of the conductance, the microwave photovoltage and the photoconductivity of GaAs samples ((A) $w = 0.5\,\mu$m, $w_{eff} \approx 0.1\,\mu$m, $L = 2\,\mu$m; (B) $w = 1\,\mu$m, $L = 2\,\mu$m) fabricated by optical lithography and RIE. In sample A, the aperiodic fluctuations of the microwave EMF (at 6.1 GHz) and of the photoconductance as a function of magnetic field were suppressed to the noise level for $B \leq 1.5\,$T. In sample B, the aperiodic oscillations of the photoconductance were superseded by SdH oscillations and not observed in strong fields, while the microwave EMF was observed also for $\omega_c\tau \gg 1$. The average period of the EMF fluctuations increased for $B > 0.5\,$T. Bykov et al calculated the autocorrelation magnetic field.

Long et al [91L2, 93L4] patterned GaAs wires ($w = 70 - 300\,$nm, $L = 10\,\mu$m) by RIE and studied their low–temperature photoresponse. The two–terminal conductance increased with time under illumination. From four–terminal conductance measurements of wires of different widths and subject to different illumination intensities, it was concluded that illumination changed the depletion depth. The decay of the photoconductance with time after removal of the illumination was examined. A high electric field ($\approx 300\,\mathrm{kVm^{-1}}$) applied to a wire for $\approx 60\,$s could reduce its conductance by many orders of magnitude. The conductance recovered some time after exposure to the high field. Long et al assumed that the light and the high electric field influenced the occupancy of traps generated by the RIE.

Klepper et al [91K3] (see page 158) fabricated GaAs wires ($w = 3\,\mu$m, $L = 22\,\mu$m, $l = 0.4\,\mu$m)

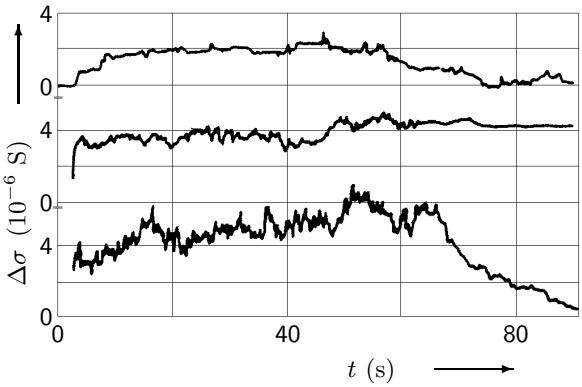

Fig. 291: Time dependence of photoconductivity at phonon flux densities (top) $n_{\mathrm{ph}} = 0.2 \cdot 10^9\,\mathrm{cm^{-2}s^{-1}}$, $1.1 \cdot 10^9\,\mathrm{cm^{-2}s^{-1}}$, and $5 \cdot 10^9\,\mathrm{cm^{-2}s^{-1}}$ (bottom) at $T = 1.7\,\mathrm{K}$ [89B4].

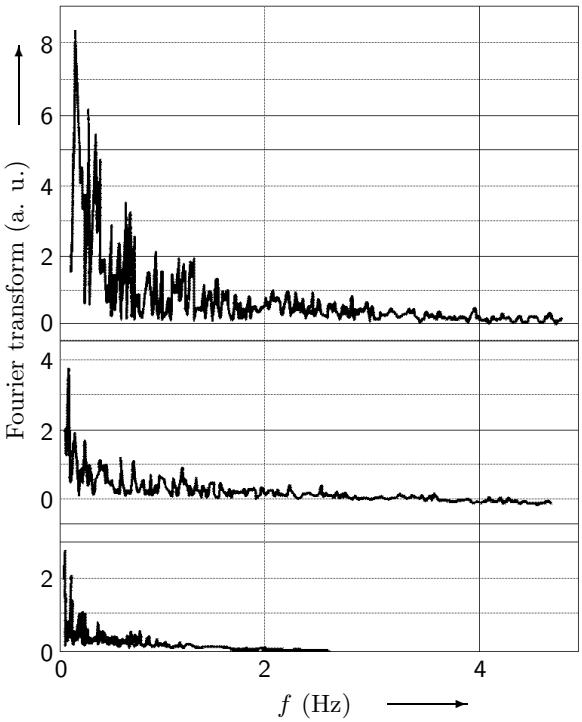

Fig. 292: Behaviour of the Fourier amplitude of the photoconductivity spectrum at light intensities (bottom) $n_{\mathrm{ph}} = 0.2 \cdot 10^9\,\mathrm{cm^{-2}s^{-1}}$, $1.1 \cdot 10^9\,\mathrm{cm^{-2}s^{-1}}$, and $5 \cdot 10^9\,\mathrm{cm^{-2}s^{-1}}$ (top) [89B4].

and studied the MC for different numbers of impurities. By IR illumination of the samples, donors in a Si–doped layer adjacent to the 2DEG were ionised, adding scatterers to the device.

Wróbel et al [92W2] measured the conductance quantization of a two–terminal GaAs wire using the time decay of the photoconductivity (see page 118).

Takaoka et al [91T1, 92T1] (see page 199) measured the non–local MR of macroscopic ($w = 20\,\mu$m, $\Delta L = 0.5\,$mm) multi–terminal GaAs wires together with the Hall resistance. The dependence on carrier concentration was examined by generating persistent photo–carriers.

11.1.2 Photovoltaic effect

In a medium without an inversion centre, illumination of a sample with an alternating field may generate a direct current even in the absence of a static electric field. This phenomenon is the *photovoltaic effect*. In thermodynamic equilibrium, fluxes of particles with opposing momenta cancel each other and thus no net current flows. When the sample is irradiated with an electric field of frequency ω, e. g. $\vec{E}\cos(\omega t)$, the fraction of particles with velocity components parallel and anti–parallel to the direction of $\vec{E}$ increases. Due to the intrinsic asymmetry of the system, the velocity distribution becomes anisotropic and a static particle current emerges.

Disordered samples lack in general an inversion centre as the impurities are randomly distributed. In a macroscopic disordered sample, the photovoltaic currents from different parts of the sample cancel each other, as the directions of the currents are random depending on the impurity configuration in the corresponding parts. This self–averaging takes place between subvolumes of size $\approx l_\varphi^3$, where l_φ is the phase coherence length. In mesoscopic conductors ($L \approx l_\varphi$) self–averaging is absent and the photovoltaic current is finite (see for example [80B, 89F4] and references therein).

Bykov et al [89B3] observed a photovoltaic effect at $6-80\,$GHz in GaAs stripes ($w = 0.5-2.0\,\mu$m, $L = 2-3\,\mu$m, $l_\varphi = 0.45\,\mu$m at $4.2\,$K). They measured the EMF induced by the microwave as a function of magnetic field and compared it with the behaviour of the MC. Reproducible oscillations were observed in both. The oscillatory EMF changed sign several times, the oscillation amplitude was of the order of the signal. The EMF fluctuations were determined by the component of the magnetic field perpendicular to the surface of the sample. Measured at different frequencies (7.1 and 77 GHz), the EMFs behaved in a similar manner. With increasing microwave power, the EMF increased approximately linearly, followed by a saturation at an EMF of $\approx 10\,\mu$V.

Bykov et al [90B3] (page 282) measured the four–probe photoconductivity of GaAs samples which oscillated aperiodically as a function of magnetic field. A value for the electron correlation energy was obtained by comparison of the amplitudes of the photoconductivity and the photovoltaic effect.

Bykov et al [91B4] (page 282) investigated the fluctuation properties of the conductance, the microwave photovoltage and the photoconductivity of GaAs samples.

11.1.3 Acoustoelectric current

A surface acoustic wave (SAW) propagating on a piezoelectric substrate generates a wave of electrostatic potential and thus interacts with the charged carriers in the system. Due to the interaction, the damping and the velocity of the surface acoustic wave change. Further, because of momentum transfer from the surface acoustic wave to the electrons, a direct current is induced into a closed circuit. This current is called *acoustoelectric current* (see for example [96S4] and references therein).

Shilton et al [96S4] reported on measurements of the acoustoelectric current induced by a SAW

($\lambda = 1\,\mu$m) in a GaAs channel defined by a split gate ($w = 0.7\,\mu$m, $L = 0.7\,\mu$m). They measured the acoustoelectric current vs. gate voltage (Figs. 293 and 294) and vs. frequency. At high SAW power levels, the acoustoelectric current existed below the pinch–off voltage. The frequency changed the current threshold value but the quantized current value on the plateau was left unchanged. The dc conductivity was measured with the SAW on and off. The presence of the SAW washed out the conductance plateaux and moved the pinch–off voltage. The dependence of the acoustoelectric current on V_g oscillated with minima corresponding to the plateaux in the channel conductivity. Shilton et al also displaced the channel sideways and examined the acoustoelectric current as a function of this displacement.

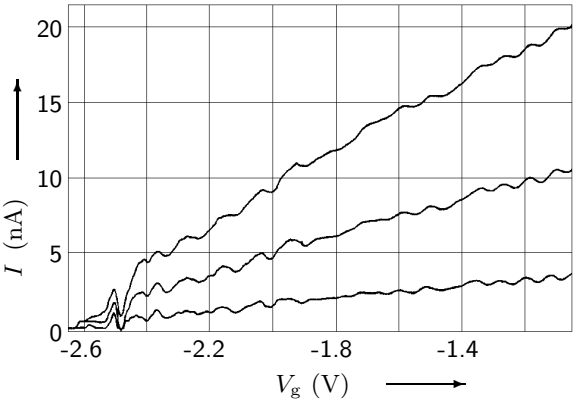

Fig. 293: Acoustoelectric current as a function of split–gate voltage for SAW powers of (top) 3 dBm, 0 dBm, and −5 dBm [96S4].

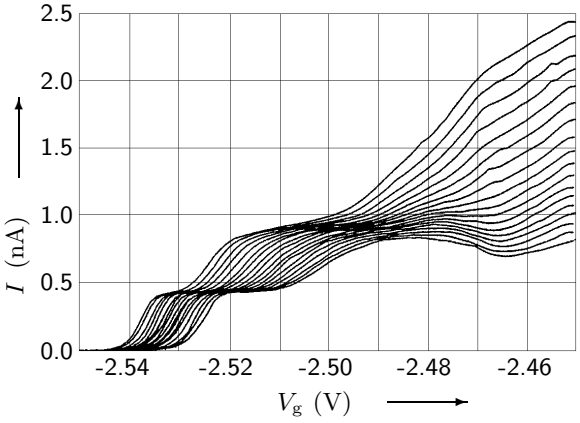

Fig. 294: Acoustoelectric current as a function of split–gate voltage beyond pinch off voltage for different values of SAW power in the range from 1.6 dBm (bottom) to 5 dBm (top) [96S4]. The SAW frequency was 2728.4 MHz.

Talyanskii et al [98T4] extended the above work of Shilton et al [96S4]. Two different GaAs wires defined by a split gate ($w = 0.7\,\mu$m, $L = 0.7\,\mu$m) were coupled to the frequencies 2728 MHz and 2886 MHz, corresponding to SAW wavelengths of $1\,\mu$m and $0.95\,\mu$m, respectively. When the channels were pinched off and the SAW power was sufficiently high, acoustoelectric currents were observed exhibiting quantized plateaux. The current values on a plateau agreed with theoretical predictions. Noise was studied and interpreted as a random telegraph signal. A peak–like structure in the acoustoelectric current was attributed to CB at an impurity–induced quantum dot inside the channel.

11.1.4 Noise

In disordered conductors, electrons suffer scattering from charged impurities located at the interface of the semiconductor heterostructure. Positively (negatively) charged impurities (acceptors and donators) may capture (emit) an electron, become neutral and be thus turned off. Neutral defects may capture or emit an electron and be thus turned on. Interference contributions to conduction in samples with $L \approx l_\varphi$ (see Section 7.2 on page 124) depend critically on the exact impurity positions. Hence, as an impurity is turned on or off, the conductance changes by an amount of the order e^2/h. Discrete jumps in conductance or resistance are observable (see for example [86M, 89K, 91F3, 97I1] and references therein).

Ralls et al [84R] observed discrete switching events in the resistance of up to 1% magnitude in a narrow Si channel. Data from a device $0.15\,\mu$m wide and $1\,\mu$m long is shown in Fig. 295. The

bottom trace in Fig. 295 shows how a $1/f$ signal can be built up by a superposition of sequences. The average times spent in the high resistance states, $\langle\tau_{on}\rangle$, and in the low resistance states, $\langle\tau_{off}\rangle$, depended exponentially on temperature and gate voltage (Fig. 296).

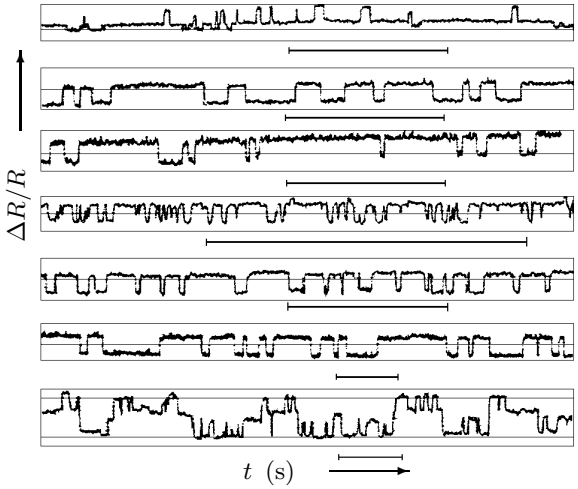

Fig. 295: Resistance switching in a particular range of temperatures and gate voltages [84R]: (top) $V_g = 13.0$ V, $T = 28$ K; 11.0 V, 28 K; 10.4 V, 28 K; 11.0 V, 34 K; 11.0 V, 30 K; 11.0 V, 26.5 K; 9.0 V, 95 K (bottom). The magnitude of the switches is of the order of 0.5% in the upper six traces and 0.2% in the bottom trace. The horizontal bars mark a duration of 5 seconds.

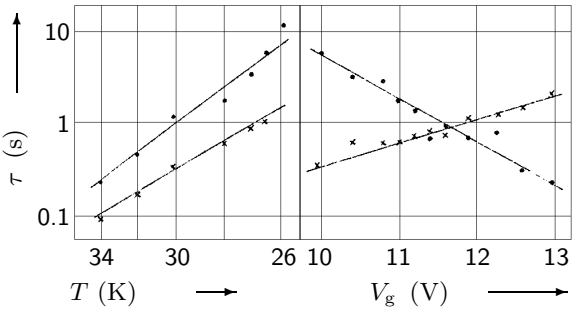

Fig. 296: Exponential dependence of mean lifetimes on temperature (left, $V_g = 11.0$ V) and gate voltage (right, $T = 28$ K) for a particular switching sequence [84R]. Dots denote $\langle\tau_{on}\rangle$, crosses $\langle\tau_{off}\rangle$.

Mankiewich et al [86M] described the fabrication of narrow multi–terminal Si MOSFETs with closely spaced probes between source and drain to enable measurements of the local voltage along the channel. The conducting channels were as narrow as 30 nm, the spacing between the probes was as close as 100 nm. The channel conductivity was measured and time–dependent voltage perturbations due to scattering at interface traps were spatially probed.

Ochiai et al [89O] observed time–dependent resistance changes in 3 μm long and nominally 0.4 μm wide AlGaAs/GaAs wires. For temperatures below 15 K, they found fast transitions between stable resistance states, the average value of the random changes was of the order e^2/h (Fig. 297). Between 15 and 200 K, the resistance exhibited fast transitions upwards followed by a slow decay. After irradiation of the sample with electron beams the resistance changes disappeared.

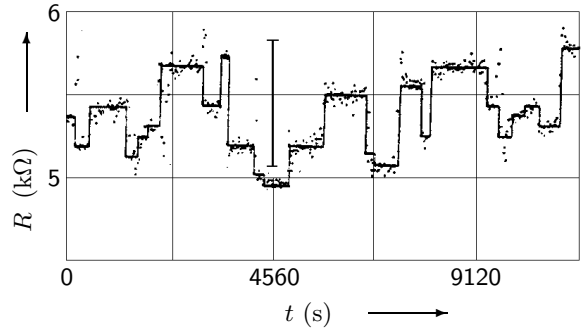

Fig. 297: Typical time–dependent resistance change at $T = 10$ K after one month [89O]. The vertical bar indicates a resistance variance of e^2/h.

Mailly et al [89M2] (see page 187) applied a voltage pulse of 0.4 V amplitude and 15 ms duration

to a 37 μm long and nominally 1 μm wide GaAs wire. The resistance increased abruptly, then decreased to its initial value within 15 minutes. Resistance jumps due to the change of the impurity potential occurred. This method was used for sample–averaging.

Bykov et al [89B4] (page 282) investigated photoconductivity in GaAs samples by exposing it to a LED. They measured $\Delta\sigma$ as a function of time, it oscillated aperiodically in time. Bykov et al discussed their results in terms of charge exchange involving a number of impurities of the order of unity.

Mailly et al [90M3] (see page 188) patterned GaAs wires by ionic etching. They applied voltage pulses to the samples causing the resistance to increase abruptly and then to decrease. The relaxation was followed by resistance jumps due to a redistribution of impurities. They measured MR for various disorder configurations.

Ohata et al [90O2] reported on the observation of random telegraph signals (RTS) in narrow poly–Si MOSFETs ((A) $w = 0.1 - 0.2\,\mu$m, $L = 10\,\mu$m; (B) $w = 0.5\,\mu$m, $L = 20\,\mu$m) at room temperature. Relative RTS amplitudes of up to 30% were observed in sample A. The relative amplitude decreased with increasing temperature or gate voltage. Ohata et al examined the autocorrelation function and measured the temperature dependence of the mean times of the high– and low–current state. In sample B, the relative amplitude of the RTSs was less than 1%. Complex RTSs with three or more levels were also observed.

Haug et al [92H1] (see page 180) fabricated narrow channels on the cleaved surface of InAs quantum well structures. At low T, some samples showed telegraph noise.

Gusev et al [92G4] (see page 190) studied two types of GaAs samples: (1) wires fabricated by EBL and (2) wires fabricated by optical lithography. In the smallest samples, switching of the resistance was observed. In samples with a stable resistance, jumps were induced by increasing the voltage. Illuminating a sample also changed the potential configuration.

Liefrink et al [94L3] examined shot noise in a GaAs wire ($w = 0.5\,\mu$m, $L = 6.2$ and $16.7\,\mu$m) defined by a split–gate. The wire was biased with a dc current, the voltage across the wire was amplified and Fourier transformed. The excess–noise spectral density was studied as a function of frequency. Below 1kHz, the noise spectra were dominated by a $1/f$ contribution. At higher frequencies, they became white.

Yamada et al [96Y2] (see page 154) fabricated GaAs wires defined by a split gate with either a small mesa in the centre of the wire or a hole near the boundary of the wire, structured using a STM. The conductance of a wire with a larger hole showed switching due to electron traps on the hole cone interface.

Smith et al [97S3] (see page 211) examined Si wires defined by side gates. The samples showed resistance switching due to single electron trapping. The step size was $\approx 50\%$ of the current value.

Jaroszyński et al [98J2] studied $Cd_{1-x}M_xTe$ wires which underwent a spin–glass transition at $0.3\,\mathrm{K} \le T_g \le 2.2\,\mathrm{K}$ for $0.07 \le x \le 0.2$. The UCF amplitude in low magnetic fields was weakly temperature dependent at $T > 0.3\,$K, but it increased abruptly below 0.3 K. An increase in the conductance noise was observed in the same temperature range. The noise was white at $T > T_g$, but behaved as $1/f^\nu$ below T_g, where $\nu = 1.3$ and 1.5 for $x = 0.07$ and 0.2 at 50 mK and $B = 0\,$T. Jaroszyński et al further examined history–dependent effects.

Talyanskii et al [98T4] (page 285) investigated SAW in GaAs wires defined by a split gate. Noise was observed and interpreted as a random telegraph signal.

Wróbel et al [98W1] fabricated GaAs wires ($w = 0.7\,\mu$m, $w_{\mathrm{eff}} = 0.28\,\mu$m, $L = 2.1\,\mu$m) by EBL and wet etching, measured MR at $T = 40\,$mK and studied in particular the conductance in the region between $\nu = 3$ and $\nu = 2$. Just below the quantized value at $\nu = 3$, G depended on time, while it was independent of time just above the quantized value at $\nu = 2$. The noise

magnitude $G - \langle G \rangle$ was $0.06 \cdot (e^2/h)$ at the lowest temperature. With increasing T, the noise magnitude decreased and the characteristic frequencies became larger. Wróbel et al showed that the conductance fluctuations were non–Gaussian.

11.1.5 Higher harmonic generation and rectification

When an ac voltage or current is applied to a system with a non–linear I–V characteristic (see Section 7.9 on page 210), higher harmonics are generated. In a conductor with an asymmetric I–V characteristic with respect to reversal of the source–drain voltage, rectification takes place (see for example [90D] and references therein).

Webbet al [85W] (see page 127) measured I–V characteristics of Si MOSFETs for several temperatures and observed a second harmonic signal.

De Vegvar et al [88dV] (see page 273) studied second harmonic generation in small rings and wires fabricated from GaAs/$Al_xGa_{1-x}As$ heterostructures.

Galloway et al [90G2] (see page 189) studied a n^+–GaAs wire ($w = 0.5\,\mu$m, $L = 9\,\mu$m) defined by EBL and dry etching. An ac voltage source was capacitively coupled to the sample and the dc voltage across the sample was measured as B was increased. Strong oscillations about zero were observed in the rectified voltage. When the applied potential was increased, the shape of the traces changed.

Brown et al [93B2, 93M2] (see page 191) examined diffusive GaAs wires ($w = 350\,$nm, $l = 40\,$nm and $\omega_c\tau = 3.3$ at $B = 18\,$T) in a local and a non–local geometry. Conductance fluctuations in a Hall geometry, rectification fluctuations, and non–local fluctuations were studied.

11.2 Lateral superlattices

11.2.1 Microwave transmission

The quasi–dc response of an array of wires is related to the transmission coefficient of microwaves irradiated onto the array. Be σ_0 the dc Drude conductivity of the system and $T(\sigma_0)$ the probability of microwaves to be transmitted through the array (at normal incidence). Then, the quantity $[T(\sigma_0) - T(\sigma_0 = 0)]/T(\sigma_0 = 0)$ is for small signals directly proportional to the real (the dissipative) part of the dynamic conductivity, $\sigma(\omega)$. Hence, measuring this quantity yields information on the transport properties of the system (see for example [87H2] and references therein).

Demel et al [88D, 89D2] (see pages 224 and 224) and Kern et al [90K1] (see page 225) measured the quasi–dc conductivity of wire arrays by microwave transmission.

11.2.2 Photoconductivity

For an introduction see Section 11.1.1 on page 282.

Demel et al [91D] (see page 225) performed magneto transport measurements on parallel GaAs wires. The MR exhibited SdH oscillations. Landau plots deviated from a linear behaviour indicating the formation of 1D subbands. The electron density could be increased by illuminating the quantum wires with short pulses from a red LED. With increasing electron density, the subband separation decreased.

Mani et al [93M3, 94M5] (see page 237) performed MR measurements on arrays of GaAs wires fabricated by holographic lithography and shallow etching. Various states of disorder were

examined using thermal annealing and the persistent photoconductivity effect.

Kreschuk et al [94K1] fabricated arrays of 10 parallel InGaAs wires ($w \approx 1.0 \pm 0.05\,\mu$m, $L =$ 2 and $10\,\mu$m) and measured the resistance vs. illumination time (of a LED). The resistance decreased by three orders of magnitude under illumination. The width of the conducting wires vs. illumination time was studied, it changed from 3 nm to 900 nm. Applying electrical impulses (of up to 10 V) caused an increase of resistance until the initial resistance was restored. By measuring the MR for several levels of persistent photoconductivity and comparing the data to weak–localization theory, the conducting channel width was determined to be $w_{\rm eff} = 30 - 58$ nm ($l_\varphi = 34 - 92$ nm).

11.3 Isolated rings

11.3.1 Complex conductance

Transport measurements on connected rings yield information on the real part of conductance, i. e. the dissipative part (see Section 10 on page 255), while the persistent current in isolated rings contains information on the imaginary part of conductance, i. e. the reactive part (see Section 9 on page 251). As contacts change a system in a fundamental manner, these components are not real and imaginary part of the same conductance, but belong to different systems. By studying the ac complex magnetic susceptibility, $\chi(\omega)$, of isolated rings one obtains both, the dissipative and the reactive part of the conductance as $\chi(\omega) = \chi'(\omega) + i\chi''(\omega) \propto i\omega G(\omega)$ in linear response. When the ac field is applied by the help of a resonator, the resonance frequency, f, and the quality factor, Q, are modified by the presence of the mesoscopic rings according to $\delta f/f = N\chi'(\omega)/V$ and $\delta(Q^{-1}) = N\chi''(\omega)/V$, where N is the number of rings and V is the volume of the resonator (see for example [94R, 94K4, 95R2, 98N2] and references therein).

Reulet et al [95R2, 98N2] measured the complex ac conductance of an array of 10^5 isolated GaAs rings ($2\,\mu$m size, $l_\varphi = 7\,\mu$m at 50 mK) fabricated by EBL. They used a resonant technique in which the rings were magnetically coupled to an electromagnetic multimode resonator whose performance was affected by the perturbations caused by the rings. They measured the magnetic–field dependence of the resonance frequency $f_1 = 310$ MHz (Figs. 298 and 299) and of the quality factor $Q = 1650$ with and without the presence of the rings in a temperature range between 10 mK and 1 K for f_1 and between 40 mK and 1 K for Q_1. The quantity $-\partial f_1/\partial H$ showed periodic oscillations corresponding to a period of $h/2e$. These oscillations were not visible for $B > 10$ G. An amplitude of the imaginary conductance of the order of $2.5 \times 10^{-3}\Omega^{-1}$ per ring was deduced. The signal increased with decreasing temperature and was fitted to an exponential law with a characteristic energy of 200 mK (Fig. 300). The data implied a diamagnetic zero–field persistent current. The quantity $\partial Q_1/\partial H$ also oscillated with a period $h/2e$ (Fig. 299). The corresponding amplitude of the real conductance was ten times greater than the $h/2e$ periodic weak–localization MC measured in identical connected rings. The quantity $\partial Q_1/\partial H$ was nearly independent of temperature until $T = 200$ mK and decreased strongly at higher T (Fig. 300). The sign of $\partial Q_1/\partial H$ was positive at small fields.

11.4 Connected rings

11.4.1 Photovoltaic effect

For an introduction see Section 11.1.2 on page 284.

In [93B5] Bykov et al had demonstrated that the AB effect could be observed via the mesoscopic photovoltaic effect. AF and periodic oscillations consistent with the AB effect had been found in the MR vs. B and in the voltage (induced by the microwave) vs. B. The relative amplitude of the

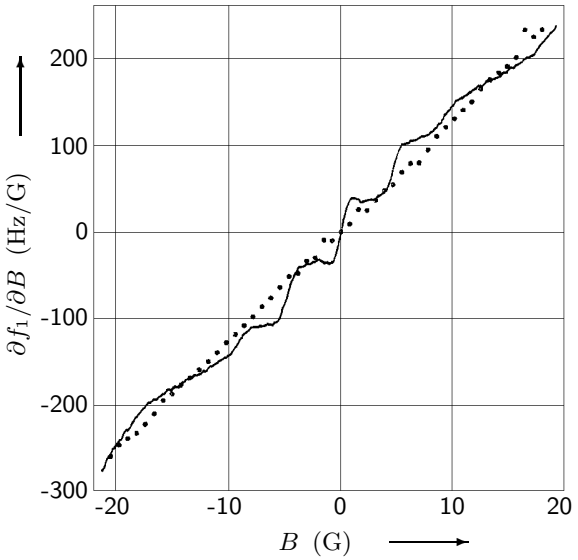

Fig. 298: Evolution of the derivative of the fundamental resonance frequency f_1 as a function of the magnetic field (full line) at $T = 55\,\mathrm{mK}$ [95R2]. The linear background (dots) was observed in the absence of the rings.

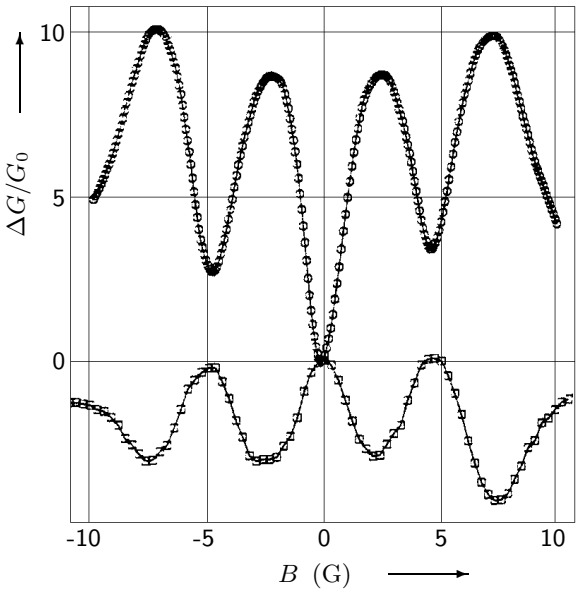

Fig. 299: Magnetic–field dependence of imaginary (top) and real (bottom, enhanced by a factor of 10) components of the conductance of the rings at $T = 55\,\mathrm{mK}$ expressed in units of the Drude conductance G_0 [95R2].

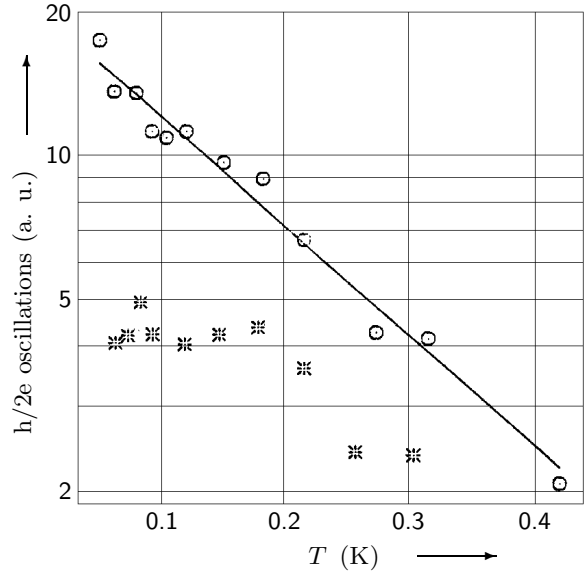

Fig. 300: Temperature dependence of the $h/2e$ periodic components of $\partial f_1/\partial H$ (circles) and $\partial Q_1/\partial H$ (stars) [95R2].

AB oscillations in the MR was 5×10^{-3}, while it was of the order of 1 in the induced voltage. This effect was then used by et al [94B1] for the examination of the influence of an electrostatic field on the AB oscillations. They prepared the samples from GaAs/AlGaAs heterojunctions. The loops were structured by EBL and RIE and had diameters of $600 - 700\,\mathrm{nm}$ and conducting widths of $15 - 60\,\mathrm{nm}$. The rings had two gates, positioned along conducting channels of the interferometer. The samples were isolating with $R > 100\,\mathrm{k\Omega}$ at gate voltages $V_{g_1} < -1\,\mathrm{V}$ and $V_{g_2} < -6\,\mathrm{V}$. The microwave power in the frequency range $8 - 12\,\mathrm{GHz}$ was fed to the samples by a coaxial cable, that in the range $37 - 80\,\mathrm{GHz}$ by a waveguide. The induced voltage was measured at temperatures $1.6 - 4.2\,\mathrm{K}$ in magnetic fields up to $1\,\mathrm{T}$, it is shown as a function of B (left) and V_{g_2} (right) in Fig. 301. The dependence on B shows periodic h/e oscillations and AF, while that on V_{g_2} shows only AF. The effect of the gate voltage on the AF and the periodic oscillations is illustrated in Fig. 302.

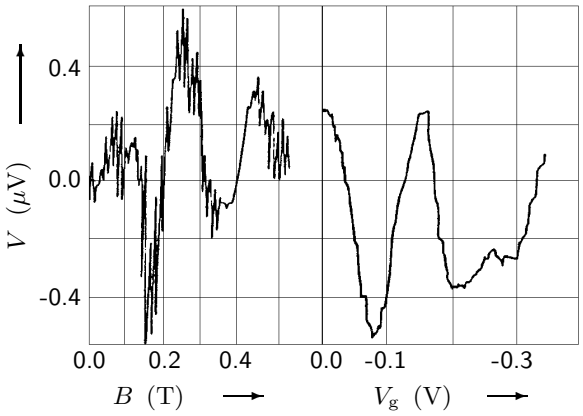

Fig. 301: Induced voltage vs. magnetic field at 9 GHz and 1.6 K (left) and vs. gate voltage on second gate at 9 GHz and 1.6 K (right) [94B1].

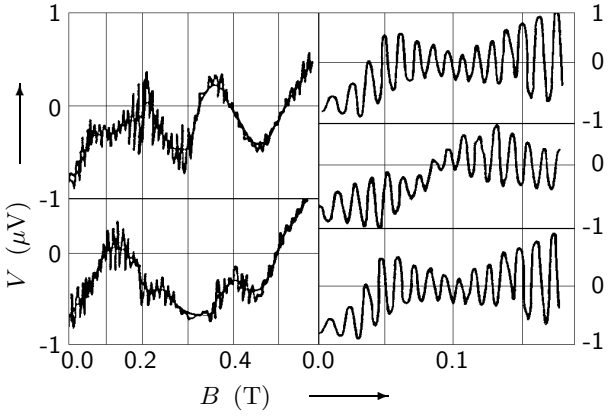

Fig. 302: Induced voltage vs. magnetic field for two different gate voltages at 9 GHz and 1.6 K [94B1] (left): $V_\mathrm{g} = 0\,\mathrm{V}$ (top) and $0.1\,\mathrm{V}$ (bottom). Reversible shift of the h/e oscillations in a magnetic field (right): $V_\mathrm{g} = 0\,\mathrm{V}$ (top), $0.1\,\mathrm{V}$ (middle), and $0\,\mathrm{V}$ (bottom).

In samples very similar to those studied in [94B1], Bykov et al found aperiodic and periodic components in the voltage (induced by the microwave field) as a function of gate voltage [95B4]. The measurements of the microwave EMF were performed at 4.2 K in magnetic fields up to 1.5 T at frequencies of $8 - 12\,\mathrm{GHz}$ fed to the sample by a coaxial cable. Periodic and aperiodic components were observed in the voltage as a function of B. The dependence on gate voltage was measured for $-0.3\,\mathrm{V} < V_\mathrm{g} < 0\,\mathrm{V}$. A gate voltage of $\approx -0.1\,\mathrm{V}$ produced a phase shift of π in the h/e oscillations. The induced voltage vs. V_g for different magnetic fields is shown in Fig. 303. The periodic component was approximately a sine curve with a period $V_\mathrm{g} \approx 0.24\,\mathrm{V}$.

Bykov et al [96B2] investigated in–plane gated InGaAs/AlGaAs rings. They measured MR in a four–probe geometry and determined the influence of V_g on the transport properties of the rings by using the microwave photovoltaic effect in the frequency range $9 - 80\,\mathrm{GHz}$. The resistance as a function of V_g showed a hysteresis explained by charge exchange of impurities in the vicinity of the 2DEG. The phase coherence length was deduced from the amplitudes of the AB oscillations measured in rings of different diameters. In a ring with a effective diameter of $0.4\,\mu\mathrm{m}$, the largest amplitude was 5% of the resistance at $T = 1.6\,\mathrm{K}$, while it was $\approx 35\%$ in a ring of effective diameter $0.7\,\mu\mathrm{m}$ at 4.2 K. The EMF vs. magnetic field exhibited a fluctuating and a periodical component (period h/e). The dependence of the EMF on V_g also contained a periodical and an aperiodical

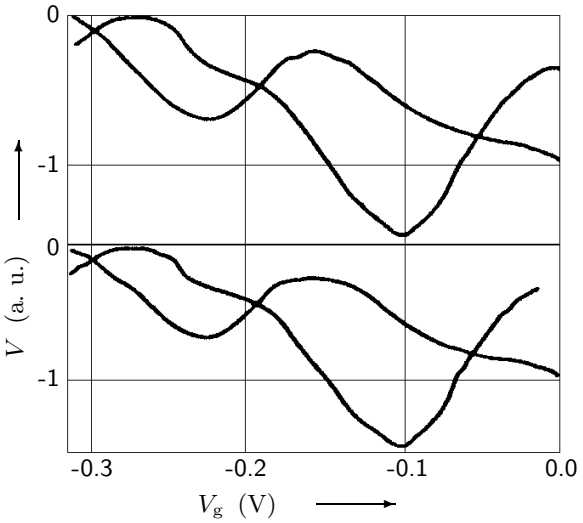

Fig. 303: Induced voltage vs. gate voltage for different values of magnetic field at 4.2 K and 9 GHz [95B4]: (right, top) $\phi = 0$, $\phi = \phi_0/2$, $\phi = \phi_0$, and $\phi = 3\phi_0/2$ (right, bottom).

component, indicating the electrostatic AB effect.

Bykov et al [98B1] investigated the photovoltaic effect in ballistic GaAs rings ($r_{\text{eff}} = 0.3 - 0.5\,\mu$m). A geometrical asymmetry of the structure was due to the fabrication technique. The resistance of the ring decreased with increasing magnetic field due to suppression of geometrical backscattering. Fluctuations with amplitudes much larger than h/e depended only weakly on temperature (at 4.2 K and 1.6 K) and were ascribed to geometrical backscattering and commensurability effects rather than interference effects. The EMF signal at 9 GHz showed h/e oscillations and aperiodic fluctuations. A correlation between $\mathrm{d}R(B)/\mathrm{d}B$ and EMF(B) was observed. For $2\hbar\omega > k_{\mathrm{B}}T$, the EMF depended strongly on frequency, in contrast to the behaviour in diffusive systems. This dependence was ascribed to geometrical effects.

Bykov et al [98B2] fabricated in–plane gated InGaAs/AlGaAs rings ($r_{\text{eff}} \approx 0.2 - 0.35\,\mu$m), applied a signal $V_0 \sin(2\pi f t)$ to one of the gate electrodes, while the other was held at a constant potential, and measured the magnetic field dependences of the differential (with respect to gate voltage) resistance and differential microwave EMF for $B \leq 2$ T at $T = 4.2$ K. They argued that the small–signal condition was fulfilled when the Fermi energy modulation due to the gate voltage did not exceed the correlation energy of the system. In this regime the gate voltage did not alter the interference pattern and the modulation technique might be used to investigate coherent processes.

11.4.2 Noise

For an introduction see Section 11.1.4 on page 285.

Mailly et al [93M1, 94M1] (page 252) observed random modifications of AB oscillations on a time scale of 10 to 40 h. These fluctuations have been associated with slow relaxation processes of the impurities in the semiconductor, inducing changes in the scattering potential or in the Fermi level.

Chandrasekhar et al [94C1] (see page 275) investigated InO rings and observed periodic oscillations of conductance as a function of gate voltage. Even though the oscillations of the conductance as a function of gate voltage were in general reproducible if the sample was kept at low temperature, the conductance of a sample occasionally changed in a discrete way, usually accompanied by a change in the pattern of the oscillations; the period of the oscillations was not affected. Chandrasekhar et al believed the discrete behaviour of the conductance to be due to the movement of

isolated impurities.

Morpurgo et al [98M] (see page 262) fabricated rings from a AlSb/InAs/AlSb heterostructure and measured the MR. The resistance showed switching events due to defects present in the heterostructure. The statistical properties of a set of $R(B)$ curves generated by the switching events was equivalent to those that would be obtained from different microscopic realizations of the same sample.

11.4.3 Higher harmonic generation

For an introduction see Section 11.1.5 on page 288.

De Vegvar et al [88dV] (see page 273) studied second harmonic generation in small rings and wires fabricated from GaAs/$Al_xGa_{1-x}As$ heterostructures.

11.5 References for Section 11

[80B] Belinicher, V.I., Sturman, B.I.: Sov. Phys. Usp. **23** (1980) 199.

[84R] Ralls, K.S., Skocpol, W.J., Jackel, L.D., Howard, R.E., Fetter, L.A., Epworth, R.W., Tennant, D.M.: Phys. Rev. Lett. **52** (1984) 228.

[85W] Webb, R.A., Hartstein, A., Wainer, J.J., Fowler, A.B.: Phys. Rev. Lett. **54** (1985) 1577.

[86M] Mankiewich, P.M., Howard, R.E., Jackel, L.D., Skocpol, W.J., Tennant, D.M.: J. Vac. Sci. Technol. B **4** (1986) 380.

[87H2] Heitmann, D.: Physics and Applications of Quantum Wells and Superlattices, NATO ASI Series B: Physics Vol. 170, edited by Mendez, E.E., von Klitzing, K. (Plenum Press, 1987).

[88D] Demel, T., Heitmann, D., Grambow, P., Ploog, K.: Appl. Phys. Lett. **53** (1988) 2176.

[88dV] de Vegvar, P.G.N., Timp, G., Mankiewich, P.M., Cunningham, J.E., Behringer, R., Howard, R.E.: Phys. Rev. B **38** (1988) 4326.

[89B3] Bykov, A.A., Gusev, G.M., Kvon, Z.D., Lubyshev, D.I., Migal', V.P.: JETP Lett. **49** (1989) 13.

[89B4] Bykov, A.A., Gusev, G.M., Kvon, Z.D., Lubyshev, D.I., Migal', V.P.: JETP Lett. **49** (1989) 135.

[89D2] Demel, T., Heitmann, D., Grambow, P., Ploog, K.: Superlatt. Microstruct. **5** (1989) 287.

[89F4] Fal'ko, V.I., Khmel'nitskii, D.E.: Sov. Phys. JETP **68** (1989) 186.

[89K] Kirton, M.J., Uren, M.J.: Adv. Phys. **38** (1989) 367.

[89M2] Mailly, D., Sanquer, M., Pichard, J.-L., Pari, P.: Europhys. Lett. **8** (1989) 471.

[89O] Ochiai, Y., Ishibashi, K., Ishida, S., Mizuno, M., Gamo, K., Kawabe, M., Murase, K., Namba, S.: Superlatt. Microstruct. **6** (1989) 337.

[90B3] Bykov, A.A., Gusev, G.M., Kvon, Z.D.: Sov. Phys. JETP **70** (1990) 742.

[90D] Datta, S., McLennan, M.J.: Rep. Prog. Phys. **53** (1990) 1003.

[90G2] Galloway, T., Gallagher, B.L., Beton, P.H., Oxley, J.P., Beaumont, S.P., Thoms, S., Wilkinson, C.D.W.: J. Phys.: Condens. Matter **2** (1990) 5641.

[90K1] Kern, K., Demel, T., Heitmann, D., Grambow, P., Ploog, K., Razeghi, M.: Surf. Sci. **229** (1990) 256.

[90M3] Mailly, D., Sanquer, M.: Surf. Sci. **229** (1990) 260.

[90O2] Ohata, A., Toriumi, A., Iwase, M., Natori, K.: J. Appl. Phys. **68** (1990) 200.

[91B4] Bykov, A.A., Gusev, G.M., Kvon, Z.D., Katkov, A.V., Plyuchin, V.B.: Superlatt. Microstruct. **10** (1991) 287.

[91D] Demel, T., Heitmann, D., Grambow, P., Ploog, K.: Superlatt. Microstruct. **9** (1991) 285.

[91F3] Feng, S.: Mesoscopic Phenomena in Solids, edited by Al'tshuler, B.L., Lee, P.A., and Webb, R.A. (Elsevier Science Publishers, 1991.

[91K3] Klepper, S.J., Millo, O., Keller, M.W., Prober, D.E., Sacks, R.N.: Phys. Rev. B **44** (1991) 8380.

[91L2] Long, A.R., Rahman, M., Kinsler, M., Wilkinson, C.D.W., Beaumont, S.P., Stanley, C.R.: Superlatt. Microstruct. **9** (1991) 35.

[91T1] Takaoka, S., Sawasaki, T., Tsukagoshi, K., Oto, K., Murase, K., Gamo, K., Namba, S.: Sol. St. Commun. **80** (1991) 571.

[92G4] Gusev, G.M., Kvon, Z.D., Ol'shanetskii, E.B.: Sov. Phys. JETP **74** (1992) 735.

[92H1] Haug, R.J., Munekata, H., Chang, L.L.: Jpn. J. Appl. Phys. **31** (1992) L127.

[92T1] Takaoka, S., Tsukagoshi, K., Oto, K., Sawasaki , T., Murase, K., Takagaki, Y., Gamo, K., Namba, S.: Surf. Sci. **267** (1992) 282.

[92W2] Wróbel, J., Kuchar, F., Ismail, K., Lee, K.Y., Nickel, H., Schlapp, W.: Surf. Sci. **263** (1992) 261.

[93B2] Brown, C.V., Geim, A.K., Foster, T.J., Langerak, C.J.G.M., Main, P.C.: Phys. Rev. B **47** (1993) 10935.

[93B5] Bykov, A.A., Kvon, Z.D., Litvin, L.V., Nastaushev, Yu. V., Mansurov, V.G., Migal', V.P., Moshchenko, S.P.: JETP Lett. **58** (1993) 543.

[93L4] Long, A.R., Rahman, M., MacDonald, I.K., Kinsler, M., Beaumont, S.P., Wilkinson, C.D.W., Stanley, C.R.: Semicond. Sci. Technol. **8** (1993) 39.

[93M1] Mailly, D., Chapelier, C., Benoit, A.: Phys. Rev. Lett. **70** (1993) 2020.

[93M2] Main, P.C., Geim, A.K., Beton, P.H., Eaves, L.: Physica B **184** (1993) 341.

[93M3] Mani, R.G., von Klitzing, K., Ploog, K.: Phys. Rev. B **48** (1993) 4571.

[94B1] Bykov, A.A., Kvon, Z.D., Litvin, L.V., Moshchenko, S.P., Nastaushev, Yu.V.: JETP Lett. **60** (1994) 809.

[94C1] Chandrasekhar, V., Webb, R.A.: J. Low Temp. Phys. **97** (1994) 9.

[94K1] Kreschuk, A.M., Kulagina, M.M., Novikov, S.V., Savel'ev, I.G., Shik, A., Kipshidze, G.D.: Superlatt. Microstruct. **16** (1994) 153.

[94K4] Kamenev, A., Reulet, B., Bouchiat, H., Gefen, Y.: Europhys. Lett. **28** (1994) 391.

[94L3] Liefrink, F., Dijkhuis, J.I., de Jong, M.J.M., Molenkamp, L.W., van Houten, H.: Superlatt. Microstruct. **16** (1994) 253.

[94M1] Mailly, D., Chapelier, C., Benoit, A.: Physica B **197** (1994) 514.

[94M5] Mani, R.G., von Klitzing, K., Vasiliadou, E., Grambow, P., Ploog, K.: Surf. Sci. **305** (1994) 654.

[94R] Reulet, B., Bouchiat, H.: Phys. Rev. B **50** (1994) 2259.

[95B4] Bykov, A.A., Litvin, L.V., Moshchenko, S.P.: JETP Lett. **61** (1995) 1005.

[95R2] Reulet, B., Ramin, M., Bouchiat, H., Mailly, D.: Phys. Rev. Lett. **75** (1995) 124.

[96B2] Bykov, A.A., Litvin, L.V., Moshchenko, S.P.: Surf. Sci. **361/362** (1996) 747.

[96S4] Shilton, J.M., Talyanskii, V.I., Pepper, M., Ritchie, D.A., Frost, J.E.F., Ford, C.J.B., Smith, C.G., Jones, G.A.C.: J. Phys.: Condens. Matter **8** (1996) L531.

[96Y2] Yamada, S., Yamamoto, M.: J. Appl. Phys. **79** (1996) 8391.

[97I1] Imry, Y.: Introduction to Mesoscopic Physics (Oxford University Press, 1997).

[97S3] Smith, R.A., Ahmed, H.: J. Appl. Phys. **81** (1997) 2699.

[98B1] Bykov, A.A., Litvin, L.V., Moshegov, N.T., Toropov, A.I.: Superlatt. Microstruct. **23** (1998) 1285.

[98B2] Bykov, A.A., Marchishin, I.V., Pogosov, A.G., Litvin, L.V., Ol'shanetskii, E.B., Gusev, G.M.: Physica B **256-258** (1998) 371.

[98J2] Jaroszyński, J., Wróbel, J., Karczewski, G., Wojtowicz, T., Dietl , T.: Phys. Rev. Lett. **80** (1998) 5635.

[98M] Morpurgo, A.F., Heida, J.P., van Wees, B.J., Klapwijk T.M., Borghs, G.: Physica B **249-251** (1998) 509.

[98N2] Noat, Y., Reulet, B., Bouchiat, H., Mailly, D.: Superlatt. Microstruct. **23** (1998) 621.

[98T4] Talyanskii, V.I., Shilton, J.M., Cunningham, J., Pepper, M., Ford, C.J.B., Smith, C.G., Linfield, E.H., Ritchie, D.A., Jones, G.A.C.: Physica B **249-251** (1998) 140.

[98W1] Wróbel, J., Jaroszyński, J., Dietl, T., Regiński, K., Bugajski, M.: Physica B **256-258** (1998) 69.2